JOURNAL OF GEOPHYSICAL RESEARCH, VOL. 105, NO. B8, PAGES 19,419–19,433, AUGUST 10, 2000

Archeomagnetism of Ontario potsherds from the last 2000 years

Yongjae Yu and David J. Dunlop

Geophysics, Department of Physics, University of Toronto at Mississauga, Mississauga, Ontario, Canada

Larry Pavlish

Archaeometry Laboratory, University of Toronto, Toronto, Ontario, Canada

Martin Cooper

Archaeological Services Inc., Toronto, Ontario, Canada

Abstract. An archeomagnetic study was carried out on potsherds samples from sites in Ontario with ages ranging from A.D. 90 to A.D. 1640 as determined by ^{14}C dating. Thellier double-heating paleointensity experiments were performed in air on 65 specimens of 52 samples from seven sample sets. Reliable paleointensity estimates were obtained for 49 specimens. Alternating field and thermal demagnetization, temperature dependence of weak-field susceptibility, and hysteresis measurements indicate that magnetite of pseudo-single-domain grain size is the carrier of natural remanent magnetization. The paleointensity results follow a half-cycle sine curve, with a steady decrease from 54.0 ± 5.9 μT to 37.6 ± 5.7 μT between A.D. 90 and A.D. 885 and a monotonic increase from 52.0 ± 6.1 μT to 59.4 ± 1.7 μT between A.D. 1200 and A.D. 1900. The paleointensities determined yield virtual axial dipole moments (VADMs) of the Earth's magnetic field that agree well with those from other parts of North America, except between A.D. 900 and A.D. 1400, when they are systematically lower. This discrepancy is probably caused by a substantial non-dipole field in southwestern North America from the tenth to the fifteenth century, since secular variation studies using potsherds from Arizona and lake sediments from Minnesota show different inclination variations during that period.

1. Introduction

Archeomagnetism is a branch of paleomagnetism applied to archeological materials. The detailed variations of absolute geomagnetic field intensity during historical times have been studied and analyzed on a global scale [e.g., *Aitken et al.*, 1989]. Although many experimental studies have been devoted to this problem, most have concentrated on sites in Europe. Relatively few archeomagnetic results have been reported from North America [e.g., *Sternberg*, 1989a]. Only three studies have been published for northeastern North America, covering 500-600 years of field variation [*Schwarz and Christie*, 1967; *Dunlop and Zinn*, 1980; *Arbour and Schwarz*, 1982]. Results of the earliest study [*Schwarz and Christie*, 1967], based on individual ceramic fragments, were reanalyzed and combined with further results by *Arbour and Schwarz* [1982].

The establishment of accurate timescales is crucial for the reliable evaluation of archeomagnetic data, since errors or deficiencies in the adopted timescales may result in false conclusions. In most cases, the basis of age dating for archeomagnetism has been provided by either archeological or historical data. Reliably calibrated radiocarbon dates have seldom been reported in archeomagnetic studies.

The present study was intended to contribute the following: (1) absolute paleointensity results spanning about 1600 years from radiocarbon-dated archeological materials sampled in Ontario in order to extend our knowledge of geomagnetic field intensity variations in northeastern North America; and (2) a record of virtual axial dipole moment (VADM) variations from the same area to test whether or not they show consistency with results from elsewhere in North America.

2. Samples

In order to identify and describe archeological resources around southern Ontario prior to site development, archeological excavations were carried out by Archaeological Services Inc. at the six sites shown in Figure 1 [*Cooper and Robertson*, 1993; *MacDonald and Williamson*, 1993; *Austin et al.*, 1994; *Williamson and MacDonald*, 1997]. Archeological assessment of each site revealed prehistoric

Paper number 2000JB900177.
0148-0227/00/2000JB900177$09.00

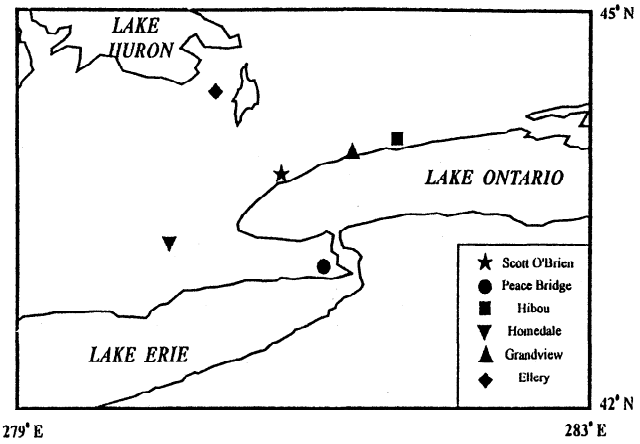

Figure 1. Schematic map showing the archeological sites sampled in this study.

settlement, with hundreds to thousands of fragments of ceramics and lithics recovered. Material from a single horizon was studied for all sites except Scott O'Brien, for which we used two sample sets, SB and SC, from horizons of widely different ages. The most detailed excavations were at the Scott O'Brien site, which provided evidence of three periods of occupation: middle Archaic (3000 B.C.), late Archaic (2500 B.C.–800 B.C.), and late Woodland (prehistoric aboriginal). The site was most intensively occupied during the Woodland period (800 B.C.–A.D. 700) [*Austin et al.*, 1994].

The substantial presence of Vinette 1 pottery and classic middle Woodland wares indicates cultural continuity. Archeological stratigraphy, changing shapes of ceramics and vessels, and changes in vegetation were used to establish relative ages. Absolute ages were provided by ^{14}C dating.

The seven sample sets, each with five or more unoriented potsherds (ceramic fragments) samples per site, have ages ranging from A.D. 90 to about A.D. 1640, as determined by ^{14}C dating using accelerator mass spectrometry at the Archaeometry Laboratory, University of Toronto (Table 1). The dating was done on charcoal and/or residues from each horizon containing pottery fragments mixed with other materials. The error limits on ages in Table 1 are $\pm 1\sigma$.

Each sample was placed in a 13.5 cm × 3.5 cm × 5.0 cm plastic container. Plaster of Paris was allowed to harden around the sample for one day in a field-free space. A 2.3-cm-diameter core was then drilled from each sample and one or two 2.0-cm-long specimens were cut from each core. The sample label and an azimuthal reference mark were scribed on top of each specimen. An arbitrary azimuthal orientation was given in order to trace directional changes in the remanence in repeated heatings. A total of 86 specimens from 57 samples were prepared (Table 1).

3. Rock Magnetic Properties

Strong-field hysteresis and the temperature dependence of weak-field susceptibility were measured to characterize the rock magnetic properties of selected samples. Room temperature hysteresis measurements in a maximum field of 0.5 T were performed on an alternating gradient force magnetometer at the University of Toronto. Hysteresis loops were obtained for 35 magnetic separates, five from each sample set. All loops were corrected for paramagnetism. Representative hysteresis loops are given in Figure 2, and hysteresis parameters of all samples measured are listed in Table 2.

Simple pseudo-single-domain (PSD) type hysteresis loops were observed in the vast majority of cases (Figures 2a, 2b, and 2c). Powder HB4 shows almost single-domain-like behavior with an M_{rs}/M_s value of 0.452 (Figure 2d). The hysteresis parameters suggest that a low-coercivity mineral is the remanence carrier. The ratios of M_{rs}/M_s and H_{cr}/H_c of the 35 separates lie in the PSD range according to the criteria of *Day et al.* [1977] (Figure 3).

To estimate Curie points, the temperature dependence of weak-field magnetic susceptibility k was determined in controlled atmospheres using a KLY-2 Kappabridge at the Institute of Rock Magnetism, University of Minnesota. Some examples are given in Figure 4. Two or three powders from each sample set were heated up to 600°C and then cooled, at a heating/cooling rate of 8°C/min. The thermomagnetic curves can be classified into three categories. Most results are of type A, characterized by nearly reversible k-T curves in both air and argon (Figure 4a). The estimated Curie point is 540-580°C, indicating magnetite or low-Ti titanomagnetite. Type B results measured in air are almost reversible, with peaks around 300°C in both heating and cooling (Figure 4b). However, in argon the peak is present only in the heating curve, with significant reduction of susceptibility in the cooling curve (Figure 4b). Samples of type C show a peak in susceptibility around 150°C in heating curves, in both air and argon (Figure 4c). The cooling curves

Table 1. The ^{14}C Ages, Locations, and Numbers of Samples

Site	Age, A.D.	Latitude, °N	Longitude, °E	n_i/N_i	n_t/N_t	n_c/N_c
Scott O'Brien 1 (SB)	90 ± 120	43.5	280.4	8/6	6/6	5/5
Scott O'Brien 2 (SC)	620 ± 60	43.5	280.4	11/7	7/7	5/5
Peace Bridge (PB)	670 ± 60	42.9	281.0	13/9	7/7	5/5
Hibou (HB)	885 ± 110	43.9	281.6	12/10	11/10	6/5
Homedale (HL)	1000 ± 50	43.2	279.7	9/7	8/6	6/5
Grandview (GA)	1425 ± 25	43.9	281.2	24/13	19/11	16/9
Ellery (ER)	1640 ±10	44.7	280.1	9/5	7/5	6/5
Total				86/57	65/52	49/39

Here n_i/N_i represents the initial number of specimens/samples prepared; n_t/N_t gives the number of specimens/samples measured; and n_c/N_c is the number of specimens/samples used in calculation.

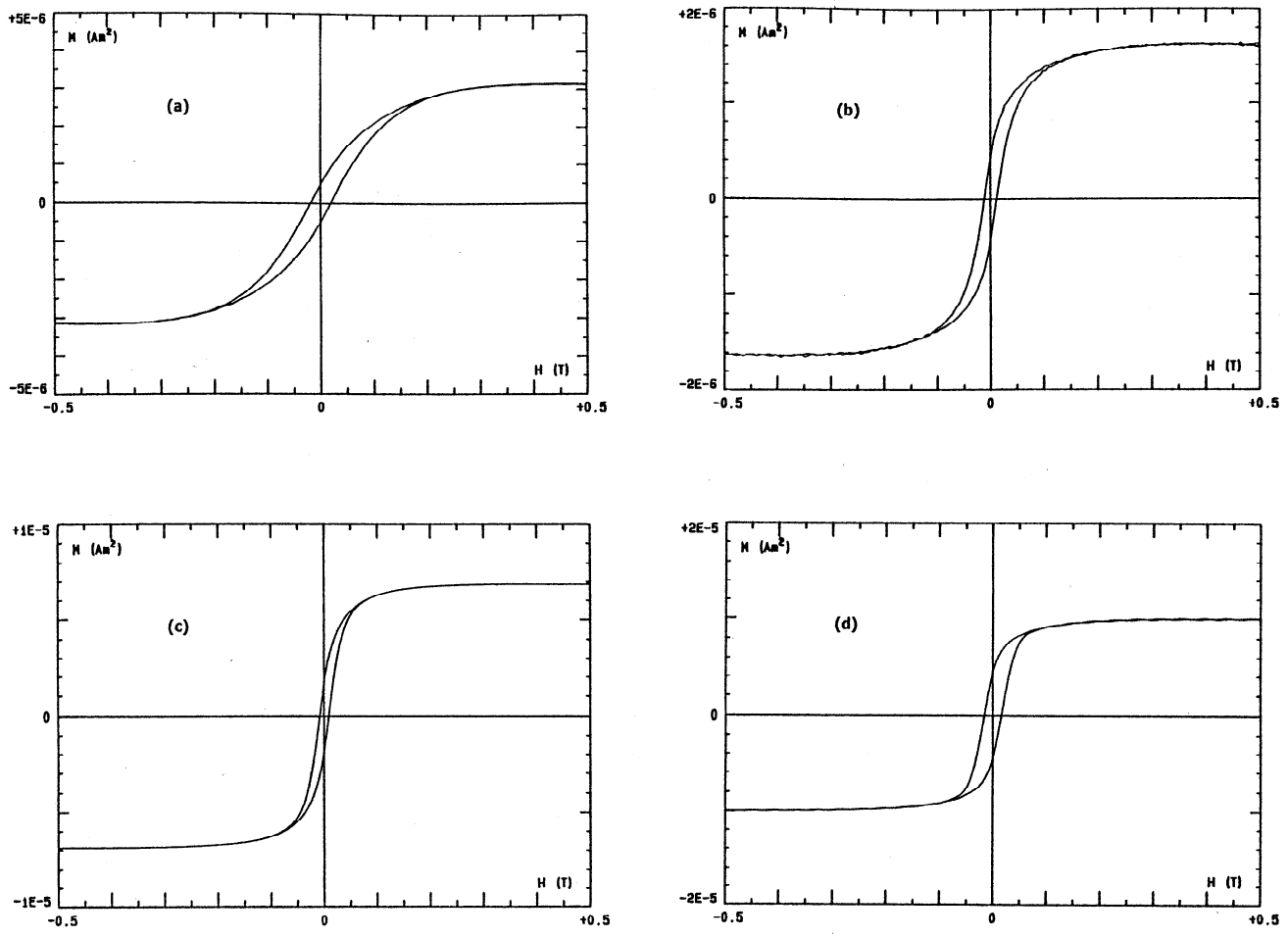

Figure 2. Examples of hysteresis loops for (a) SB1, (b) SC5, (c) ER3, and (d) HB4.

obtained in air show enhancement of susceptibility over the entire temperature range, resulting in differences between heating and cooling curves. In argon the cooling curve below 330°C is much lower than the heating curve.

It is surprising that samples of types B and C show more reversible thermomagnetic behavior in air than in argon atmosphere. Significant reductions of susceptibility for type B and C samples when heated in Ar seem to indicate alteration from magnetic to nonmagnetic or weakly magnetic phases. It is not clear why the same changes do not occur during heatings in air.

4. Paleointensity Experiments

Of the 86 specimens prepared, eight specimens were used for alternating field (AF) demagnetization, and 13 specimens fractured and became unusable during thermal demagnetization. The remaining 65 specimens used in paleointensity experiments were divided into 11 sets of six specimens, the maximum number that could be accommodated in the furnace at one time. The six specimens in each set were chosen to have similar intensities of natural remanent magnetization (NRM). Each heating-cooling-measurement step required 1.5 to 2 hours. Specimens were heated and cooled twice from each temperature T, the first cooling being in zero field to demagnetize part of the NRM and the second cooling being in a known laboratory field to impart partial thermoremanent magnetization (pTRM).

A modified version [*Coe*, 1967] of the Thellier method [*Thellier and Thellier*, 1959] was applied as follows. After the first (zero-field) heating-cooling step to temperature T_i, the remanence was measured, and the NRM lost was calculated by vector subtraction of the previous remanence. The second heating-cooling step to temperature T_i was in H_{lab} = 20 ± 0.13 μT along the cylindrical axis of the specimen. During pTRM acquisition experiments, calibration of the applied field was rechecked at every thermal step. The pTRM acquired was calculated by vector differencing of the remanences measured after the two heating-cooling steps. Double heatings and coolings were performed in 50°C steps from 100°C to 500°C and then in 40°C steps to 580°C, using a Schonstedt TSD-1 furnace. Temperatures were reproducible within ±2°C. All the measurements were performed in air. The residual field in the heating (cooling) chamber of the furnace, which was measured at least once per day, was 80-200 nT (5-40 nT).

In an attempt to reduce possible alteration the samples were held at high temperature for only 15 min (required minimum time since the thermal diffusivities of baked clays and plaster of Paris are of the order of 10^{-7} m^2/s). It required 10–20 min to heat cold specimens up to the target temperature, where they were then held for 15 min before

Table 2. Hysteresis Properties

Site	Sample	M_s, μA m^2	M_{rs}, μA m^2	M_{rs}/M_s	H_c, mT	H_{cr}, mT	H_{cr}/H_c
SB	1	3.13	0.493	0.157	19.1	42.3	2.22
	2	0.073	0.017	0.237	7.07	15.5	2.19
	4	0.210	0.037	0.175	8.85	23.2	2.62
	5	0.176	0.041	0.232	9.12	19.5	2.14
	6	0.206	0.041	0.202	9.22	18.9	2.05
SC	1	13.5	3.44	0.255	11.1	25.0	2.25
	4	1.23	0.316	0.257	11.2	22.5	2.01
	5	1.62	0.444	0.274	11.9	24.4	2.05
	7	0.390	0.043	0.109	8.64	33.6	3.89
	8	0.191	0.051	0.269	16.4	36.8	2.24
PB	3	1.44	0.346	0.239	7.37	16.4	2.23
	4	8.64	2.28	0.264	9.85	19.7	2.00
	6	1.27	0.342	0.270	7.63	16.5	2.16
	8	3.71	1.05	0.283	8.56	18.1	2.11
	9	0.054	0.010	0.190	7.08	18.2	2.57
HB	1	0.525	0.156	0.297	13.7	25.2	1.84
	2	7.06	1.81	0.256	7.91	20.1	2.54
	4	9.93	4.49	0.452	16.3	26.4	1.62
	6	13.3	4.66	0.351	11.5	20.4	1.77
	10	14.2	3.97	0.279	8.83	24.3	2.75
HL	2	33.5	9.99	0.300	8.43	20.7	2.46
	3	8.43	1.48	0.176	7.16	17.5	2.44
	4	1.77	0.453	0.255	7.58	16.3	2.15
	6	1.88	0.468	0.249	6.36	11.2	1.76
	7	1.89	0.446	0.236	7.94	18.7	2.36
GA	1	0.255	0.079	0.310	22.6	45.7	2.02
	2	1.07	0.260	0.242	10.6	22.5	2.12
	15	8.94	1.72	0.193	10.4	22.4	2.15
	16	6.07	1.42	0.235	7.33	16.5	2.25
	17	3.02	0.666	0.220	8.11	17.4	2.15
ER	1	10.2	2.31	0.227	5.48	13.0	2.37
	3	6.87	1.84	0.267	8.91	17.4	1.95
	4	2.52	0.423	0.168	8.49	21.6	2.54
	5	9.43	1.77	0.188	3.86	12.7	3.29
	6	5.15	1.36	0.263	6.30	14.9	2.37

Five different powders were obtained from five different samples per site. Values of saturation magnetization (M_s), saturation remanence (M_{rs}), and coercive force (H_c) were determined from hysteresis loops. Values of remanence coercivity (H_{cr}) were obtained from backfield measurements.

cooling. To monitor possible chemical alteration, bulk magnetic susceptibility was measured after each heating step. Two pTRM checks were made, at 300°C and 400°C.

5. Results

5.1. AF and Thermal Demagnetization

One specimen per site was AF demagnetized in 12 steps up to 100 mT using a Schonstedt GSD-1 AF demagnetizer. About 10% of the NRM intensity remains after demagnetization to a peak field of 80 mT. Median destructive fields are 30-40 mT. The NRM vector is stable in direction throughout AF treatment (Figure 5a).

Typical thermal demagnetization results are shown in Figure 5b, along with the variation of bulk susceptibility resulting from repeated heatings. In most cases a viscous component was removed below 200°C. The distributed unblocking temperatures observed in thermal demagnetization, with a maximum unblocking temperature of 580°C, suggest PSD magnetite as the remanence carrier [*Dunlop and Özdemir*, 1997].

5.2. Paleointensity Results

Altogether, 65 specimens from 52 samples were used in paleointensity experiments. The paleointensity values were obtained from the slope of the Arai plot [*Nagata et al.*,

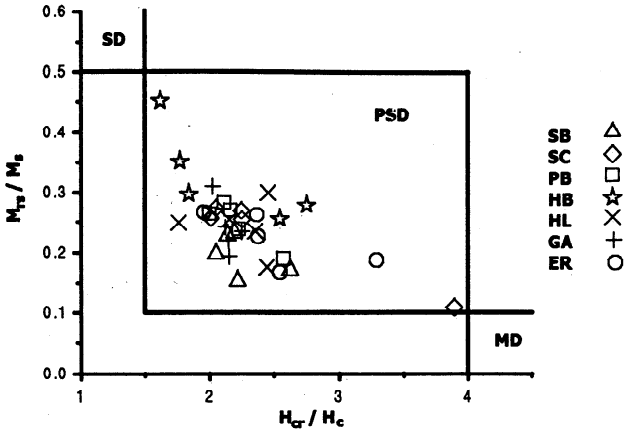

Figure 3. Hysteresis parameters for our samples on a Day plot. SD, single domain; PSD, pseudo-single-domain; MD, multidomain.

1963], which gives the ratio between ancient geomagnetic field H_{nature} and applied laboratory field H_{lab}. Paleointensity estimates were accepted only when both pTRM checks and bulk susceptibility values showed <5% difference with the initial pTRMs and the susceptibility of the previous steps, respectively. Ten specimens were rejected according to these criteria. Final reliable paleointensity estimates are summarized with their statistical parameters in Table 3.

To describe the quality of an individual paleointensity determination, we must evaluate several factors. The remanence fraction parameter f and the gap factor g measure what fraction of total remanence was utilized and how evenly the data points were distributed [*Coe et al.*, 1978]. For details concerning the definitions of the new quality factor S' and weighting factor w, statistical methods used, and the statistical rejection criteria, refer to Appendix A. Six specimens, identified by parentheses in Table 3, were excluded from the averaging because of their high S' values. Two averages are given for each site in Table 3: a weighted mean paleointensity, obtained by weighting each H_e value by its corresponding w value, and an unweighted mean, obtained by simply averaging the H_e values of all specimens.

The standard deviation in the estimated paleointensity for each site is ~10%. The weighted and unweighted estimates of paleointensity and VADM agree within these error limits. Most results from multispecimen samples, such as GA17-1, -2, and -3, show good coherency both in the temperature ranges over which linearity was observed and in estimated paleointensities.

5.3. Behavior in Arai Plots

Figure 6 shows one example per site of Arai plots reflecting typical paleointensity results. Specimens SC1 of Scott O'Brien (Figure 6a) and HB2-1 of Hibou (Figure 6b) yielded ideal behavior in their NRM-TRM curves over nine steps from 200°C to 580°C, spanning 87% and 89% of the total NRM, respectively. They also show good quality (S' <1) in line fitting and have excellent repeatability of pTRM checks. Clear one-component decay of NRM was also evident in vector projections.

Results with similar linearity, but over more limited ranges of temperature and NRM fraction, were obtained for SB5 of Scott O'Brien (Figure 6c) and HL6 of Homedale (Figure 6d). Well-defined leastsquares segments were defined by eight points between 200°C and 540°C, with overall good quality as indicated by S', pTRM checks, and univectorial behavior in vector plots. Reduction of f values (to ~65%) in these specimens is caused by the unused point at 580°C and the resulting reduction in the fraction of NRM utilized. About 30% of the NRM demagnetizes between 540°C and 580°C in these specimens.

Specimens GA15-1 of Grandview (Figure 6e), ER3 of Ellery (Figure 6f), and PB6 of Peace Bridge (Figure 6g) show two distinct segments of different slopes. The steeper slope occurs in lower temperature (200-450°C) ranges and the shallower slope in high temperature ranges (450-580°C). Two different components were also detected in vector projections. The second component is not so obvious for specimen PB6 because it has a similar direction to the low-temperature vector. In these specimens, no notable bulk susceptibility changes were detected during heating experiments. This fact suggests that irreversible chemical changes are not the cause of the change in slope of the Arai plots. Either these potsherds were heated twice (an initial heating up to the Curie temperature of magnetite and a second heating up to 450°C) or else the potsherds were initially heated only up to 450°C.

If the samples had been heated twice during prehistoric times, the slopes should not differ by more than a factor of 2, since the geomagnetic field intensity has not varied more than a factor of 2 during the past 2000 years [*Aitken et al.*, 1989]. Greater differences in slopes, as observed for GA15-1, ER3, and PB6, suggest that the shallow slope of NRM-TRM curves at high temperatures represents an artefact resulting from laboratory heating through a range where no NRM was originally acquired. Thus the shallow slopes at higher temperatures probably do not record an ancient magnetic field. In the case of dual segments the slope calculation for paleointensity determination was performed using the segment below 400-500°C. A similar interpretation and procedure were adopted for Quebec potsherds by *Arbour and Schwarz* [1982] and for Hohokam potsherds by *Sternberg* [1989b].

Some of pTRM checks are remarkably good and are indistinguishable from the earlier pTRMs within the size of symbols used in the diagrams (e.g., Figures 6d and 6g). This is independent evidence that the shallow high-field slopes do not result from sample alteration above 450°C but from lack of original NRM in this temperature range.

5.4. Paleointensity and VADM as a Function of Age

The site-mean absolute paleointensity values have been plotted in Figure 7 as a function of age of the samples. Data of *Dunlop and Zinn* [1980] from the Jordan kiln, Ontario, and *Arbour and Schwarz* [1982] from Pointe du Buisson, Quebec, are also plotted, using different symbols. It is notable that results of similar age in this study and other studies [*Dunlop and Zinn*, 1980; *Arbour and Schwarz*, 1982] are consistent with each other within their error ranges, although there are large uncertainties in age for the potsherds of *Arbour and Schwarz* [1982]. The combined paleointensity

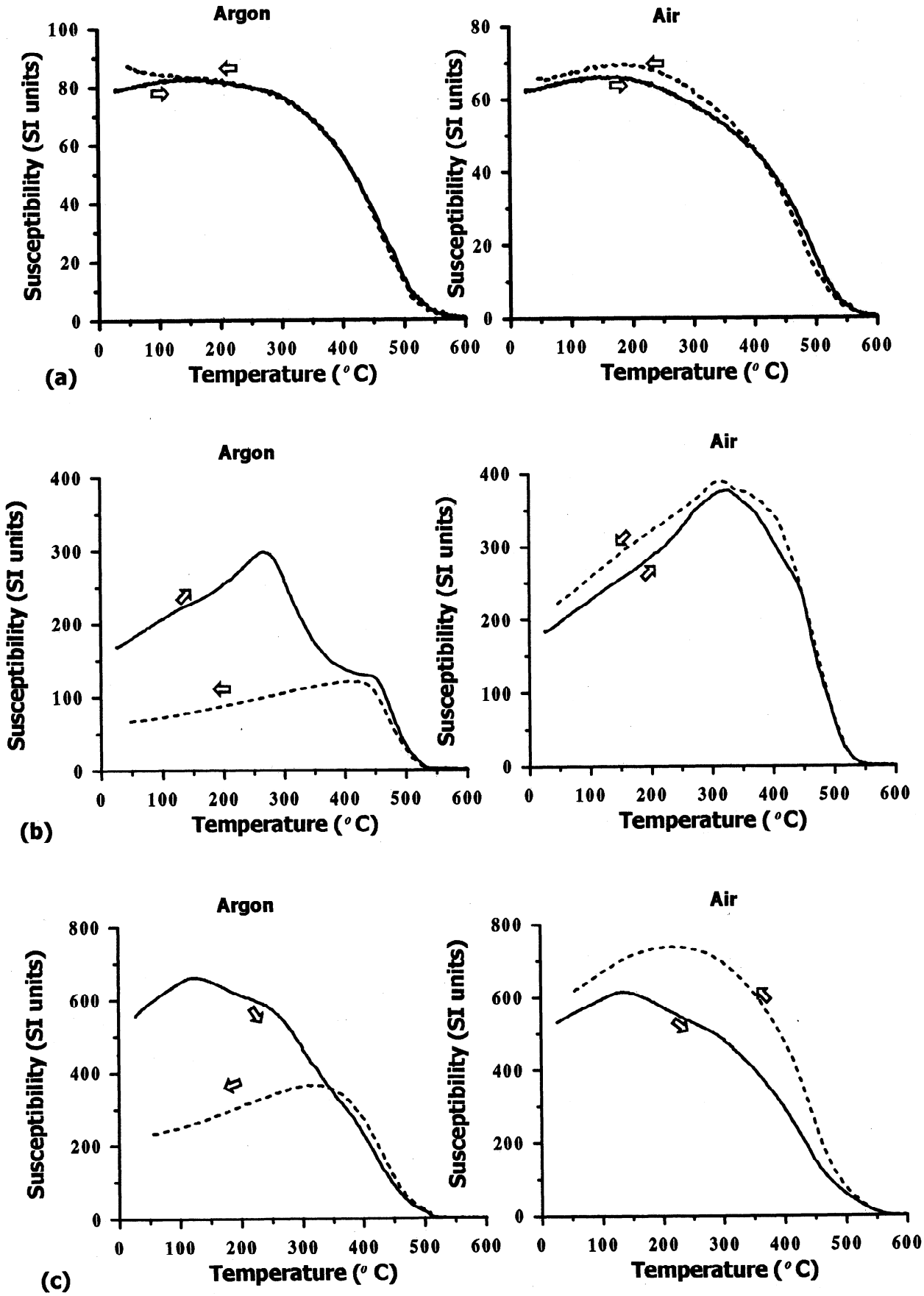

Figure 4. Examples of thermomagnetic curves for (a) GA 17, (b) HB4, and (c) ER1. Solid (dashed) lines are for heating (cooling).

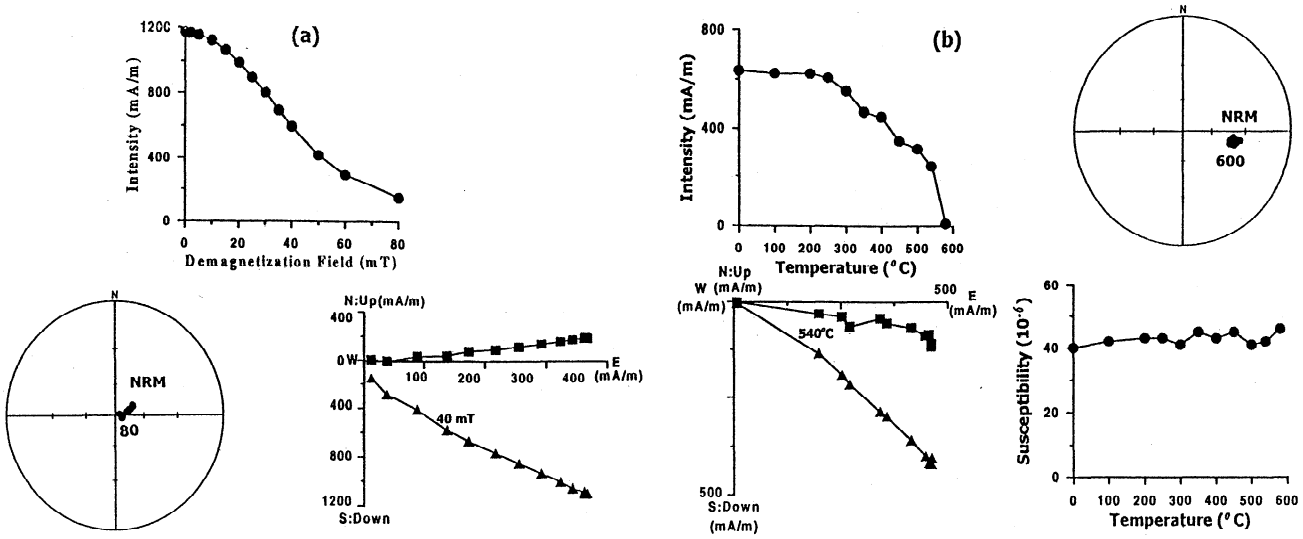

Figure 5. Examples of AF and thermal demagnetization results for (a) HL5 AND (b) GA11. Total intensity decay of magnetization, an equal-angle stereographic plot, and vector projections are shown for each sample. Bulk susceptibility values after each heating are also plotted with the thermal demagnetization results. Open and solid circles represent upper and lower hemisphere unit vectors, respectively. Squares and triangles are horizontal and vertical plane projections, respectively.

Table 3. Paleointensity Results [a]

Specime n	N	ΔT, °C	f	g	σ_a, 10^{-2}	σ_b, 10^{-1}	S'	w, 10^2	$H_e \pm \sigma_{He}$, μT	$H_a \pm \sigma_{Ha}$, μT	VADM, 10^{22} A m^2
SB1	6	300-540	0.66	0.63	3.37	3.45	0.38	0.58	59.06 ± 6.92		
SB2	9	200-580	0.76	0.69	4.04	1.94	1.92	0.48	63.98 ± 3.89		
SB4	8	200-540	0.74	0.85	2.45	1.13	2.63	1.40	44.43 ± 2.28		
SB5	8	200-540	0.65	0.84	2.20	1.14	1.21	1.97	42.17 ± 2.29		
SB6	8	200-540	0.68	0.83	3.39	3.49	0.10	1.54	72.67 ± 7.00		
										53.95 ± 5.94 [b]	8.97 ± 0.99 [b]
										56.46 ± 5.81 [c]	9.38 ± 0.97 [c]
SC1	9	200-580	0.87	0.86	2.28	1.69	0.33	3.36	39.33 ± 3.44		
SC4	9	200-580	0.88	0.79	2.79	1.55	0.30	2.95	58.41 ± 3.16		
SC5	5	200-400	0.46	0.69	5.44	3.67	0.21	0.35	65.13 ± 7.34		
SC7	6	200-450	0.44	0.79	3.42	2.45	0.39	0.66	47.40 ± 4.91		
SC8	6	200-450	0.39	0.78	3.33	2.71	0.31	0.61	47.51 ± 5.42		
										48.85 ± 4.75 [b]	8.12 ± 0.79 [b]
										51.56 ± 4.55 [c]	8.57 ± 0.76 [c]
(PB2)	6	200-450	0.56	0.74	2.99	0.83	3.39		(35.60 ± 1.67)		
PB3	6	200-450	0.45	0.78	3.39	2.73	1.14	0.35	51.01 ± 5.48		
PB4	6	200-450	0.63	0.75	2.66	0.96	1.28	1.64	36.44 ± 1.94		
PB6	6	200-450	0.60	0.77	4.20	1.82	0.48	0.87	55.09 ± 3.56		
PB8	6	200-450	0.45	0.72	4.10	4.08	0.27	0.37	64.39 ± 8.16		
PB9	6	200-450	0.56	0.78	2.26	1.04	1.10	1.77	33.30 ± 2.09		
										41.64 ± 6.64 [b]	6.97 ± 1.11 [b]
										48.05 ± 5.82 [c]	8.04 ± 0.97 [c]

Table 3. (continued)

Specimen	N	ΔT, °C	f	g	σ_a, 10^{-2}	σ_b, 10^{-1}	S'	w, 10^{2}	$H_e \pm \sigma_{He}$ μT	$H_a \pm \sigma_{Ha}$ μT	VADM, 10^{22} A m^2
HB1	7	200-500	0.44	0.81	2.67	1.03	0.65	1.58	30.21 ± 2.08		
HB2-1	9	200-580	0.89	0.83	2.27	0.84	0.75	4.43	43.09 ± 1.72		
HB2-2	9	200-580	0.97	0.81	1.91	0.89	0.87	4.95	42.46 ± 1.80		
HB4	7	200-500	0.46	0.79	2.37	0.74	2.37	1.33	26.44 ± 1.49		
(HB5)	7	200-500	0.54	0.71	2.97	1.00	5.09		(37.38 ± 2.01)		
HB6	7	300-580	0.97	0.77	1.51	0.97	1.62	4.02	27.61 ± 1.97		
(HB7)	9	200-580	0.96	0.82	1.88	0.70	2.81		(37.49 ± 1.43)		
HB10	7	200-500	0.64	0.74	3.75	2.73	0.44	0.70	62.68 ± 5.48		
										37.56 ± 5.66 [b]	6.21 ± 0.94 [b]
										38.75 ± 5.64 [c]	6.41 ± 0.93 [c]
(HL1)	7	200-500	0.72	0.76	1.67	0.39	6.27		(23.37 ± 0.80)		
HL2	7	200-500	0.70	0.81	3.01	1.77	0.58	1.42	53.59 ± 3.55		
HL3	6	200-450	0.28	0.57	4.66	2.40	0.54	0.19	39.81 ± 4.81		
HL4-1	6	200-450	0.61	0.78	4.59	4.12	2.91	0.15	68.69 ± 8.26		
HL4-2	6	200-450	0.54	0.78	5.30	4.93	1.73	0.12	77.50 ± 9.87		
HL6	8	200-540	0.64	0.83	2.66	1.41	1.30	1.24	47.53 ± 2.83		
HL7	5	200-400	0.47	0.72	5.05	2.90	0.79	0.26	52.63 ± 5.81		
										52.02 ± 6.05 [b]	8.67 ± 1.01 [b]
										56.63 ± 5.69 [c]	9.44 ± 0.95 [c]
GA1-1	8	200-540	0.79	0.82	3.17	2.23	0.47	1.33	66.56 ± 4.49		
GA1-2	8	200-580	0.99	0.79	2.71	2.00	0.45	2.18	65.64 ± 4.02		
GA2-2	8	200-580	1.00	0.77	2.41	1.77	0.91	1.90	60.66 ± 3.56		
GA2-3	6	350-580	0.93	0.79	3.16	1.94	0.37	1.92	53.40 ± 3.90		
GA3	7	300-580	0.98	0.78	1.64	1.01	0.91	4.82	26.63 ± 2.04		
GA4-1	6	200-450	0.64	0.71	2.86	1.16	0.48	1.97	41.29 ± 2.33		
GA4-2	6	200-450	0.63	0.73	3.61	1.75	0.97	0.74	51.44 ± 3.51		
GA5	5	250-450	0.46	0.73	3.21	0.47	0.40	3.59	57.78 ± 7.84		
GA11	8	200-540	0.57	0.82	2.94	1.82	1.36	0.75	51.34 ± 3.66		
(GA12)	8	200-540	0.69	0.81	2.21	1.06	3.78		(42.81 ± 2.14)		
GA15-1	6	200-450	0.47	0.79	9.58	5.40	0.61	0.09	83.90 ± 10.82		
GA15-2	6	200-450	0.56	0.75	5.61	0.30	1.80	1.86	59.51 ± 4.84		
GA16-1	9	200-580	1.00	0.83	1.72	1.16	0.78	4.72	38.47 ± 2.36		
GA16-2	9	200-580	1.00	0.85	2.18	1.04	0.33	6.48	47.72 ± 2.11		
GA17-1	7	200-500	0.53	0.81	2.49	1.63	1.00	1.06	40.38 ± 3.26		
GA17-2	7	200-500	0.54	0.81	2.81	1.65	0.63	1.18	43.00 ± 3.30		
GA17-3	7	200-500	0.51	0.80	2.67	1.58	1.03	0.95	41.95 ± 3.17		
										47.43 ± 3.64 [b]	7.85 ± 0.60 [b]
										51.85 ± 3.45 [c]	8.58 ± 0.57 [c]
ER1	6	200-450	0.48	0.76	6.20	2.34	0.53	0.35	59.17 ± 4.70		
ER3	6	200-450	0.68	0.79	4.46	1.66	1.10	0.68	55.37 ± 3.34		
(ER4-1)	6	200-450	0.73	0.73	3.56	1.07	4.96		(48.55 ± 2.17)		
ER4-2	6	200-450	0.74	0.76	4.49	1.65	0.68	0.92	59.49 ± 3.32		
ER5	5	200-400	0.57	0.58	5.14	1.61	1.52	0.33	53.54 ± 3.24		
ER6-1	6	350-580	0.82	0.51	3.44	1.94	1.05	0.61	58.47 ± 3.90		
ER6-2	6	350-580	0.77	0.62	4.28	2.20	0.36	0.85	65.41 ± 4.42		

Table 3. (continued)

Specimen	N	ΔT, °C	f	g	σ_a, 10^{-2}	σ_b, 10^{-1}	S'	w, 10^2	$H_e \pm \sigma_{He}$ μT	$H_a \pm \sigma_{Ha}$ μT	VADM, 10^{22} A m^2
										59.37 ± 1.71 [b]	9.74 ± 0.28 [b]
										58.58 ± 1.67 [c]	9.61 ± 0.27 [c]

[a] N is the number of points used in paleointensity determination; ΔT is the interval of temperature used in slope calculation; f and g are NRM fraction and gap factor, respectively [*Coe et al.*, 1978]; S' and w are the quality factor and the weighting factor defined in Appendix A; σ_a and σ_b are the standard errors in the y intercept and the slope [*York*, 1969]; H_e is the estimated paleointensity of each specimen and σ_{He} is the standard error from leastsquares fitting; H_a is the weighted average paleointensity of each site and σ_{Ha} is the standard deviation associated with the weighted average; samples whose numbers and H_e values are in parentheses were not used in the averaging because their values were higher than the 99% confidence limits in Table 4.

[b] weighted means of estimated paleointensities and VADMs.

[c] unweighted means of estimated paleointensities and VADMs.

results from southern Ontario and Quebec are in excellent agreement with relative paleointensity results obtained from Lake Le Boeuf, Pennsylvania [*King et al.*, 1983].

Within the limits imposed by the number of sites, the results seem to trace about a half cycle of a sine-shaped curve, with a broad minimum centered on the tenth century, when the estimated Earth's magnetic field intensity in southern Ontario was around 40-50 μT (Figure 7). The intensity decreased between A.D. 90 and A.D. 885. The results also suggest a monotonic increase in paleointensity between A.D. 1200 and A.D. 1900 with a slight hump around A.D. 1000. A generally similar pattern of intensity variations was reported by *Sternberg and Butler* [1978] and *Sternberg* [1989a] for potsherds from the American Southwest.

In order to compare paleointensity values from areas at different latitudes, VADMs were calculated from the weighted mean paleointensities. Results are plotted and compared with the results from *Sternberg* [1989a] and *Dunlop and Zinn* [1980] in Figure 8. Results from southwestern U.S. archeointensities [*Lee*, 1975; *Parker*, 1976], Holocene igneous rocks [*Champion*, 1980], Quebec potsherds [*Arbour and Schwarz*, 1982], and Hohokam potsherds from Arizona were compiled and analyzed by *Sternberg* [1989a]. Horizontal error bars represent uncertainty in age, and vertical error bars represent the standard error of the mean VADM (Figure 8).

6. Anisotropy of Anhysteretic Remanence

Although standard deviations of estimated paleointensities are no more than 10% for most sites, there are some individual sample values that deviate considerably from the mean. We have little information about prehistoric pottery-making technology in Ontario, but one possible source of scatter is magnetic fabric anisotropy [*Rogers et al.*, 1979; *Sternberg*, 1989a].

Because of the many repeated heatings required to determine anisotropy of TRM, we used instead anisotropy of anhysteretic remanent magnetization (AARM) [*Jackson et al.*, 1988], which causes no chemical alteration of the samples. ARMs were produced in six successive directions ($\pm x$, $\pm y$, $\pm z$) to obtain the AARM tensor. ARM was imparted with a Schonstedt AF demagnetizer in a peak field of 100 mT, with an added steady field of 20 μT. Anisotropy degree P_J and shape parameter T [*Jelinek*, 1981] were calculated from the principal anisotropy components (diagonal terms of the AARM matrix) to define the characteristics of the AARM anisotropy ellipsoids. Most samples have oblate ellipsoids ($T>0$), with relatively small anisotropy. Only six specimens have P_J larger than 1.2. (Figure 9). There is no correlation between the degree of anisotropy and the estimated paleointensity value H_e in Table 3. Therefore magnetic fabric anisotropy is not an important factor in this study.

7. Discussion

7.1. Paleointensity Determination

Although the effect of coolingrate differences on TRM intensity has been debated theoretically [*Dodson and McClelland Brown*, 1980; *Halgedahl et al.*, 1980] and investigated experimentally [*Fox and Aitken*, 1980], the effect of differences in natural and laboratory cooling rates is likely to be small for pottery. Therefore no coolingrate correction was applied in slope calculation.

Some of our Arai plots have two segments of different slopes, giving an overall convex-down shape (Figures 6e, 6f, and 6g). One mechanism for such behavior, the presence of multidomain (MD) grains [*Levi*, 1977], is probably not relevant in this study. To investigate the grain size of magnetic minerals, magnetic powders were extracted by gently crushing small fragments of samples. Octahedral magnetite grains were observed under a stereoscopic microscope. All individual magnetite grains were smaller than 10 μm in diameter. PSD grain sizes (≤10 μm for magnetite) were also inferred from AF and thermal demagnetization and hysteresis measurements (see sections 3 and 5.1). Note that magnetite grains have to be larger than 10 μm in size to exhibit significantly curved Arai plots due to MD behavior [*Dunlop and Özdemir*, 1997].

Out of 49 specimens, 22 show ideal behavior in the Arai plot (e.g., Figures 6a and 6b). Most points between 200°C and the highest blocking temperature lie on a good straight line. The other 27 specimens show two slopes in the Arai plot, a steeper slope in lower temperature ranges and a shallow slope in higher temperature ranges. This flattening is likely an artefact resulting from a sample with no prior NRM above 450°C acquiring a small remanence during "zero-field" steps. The field intensity estimated from the shallow slope is ~5 μT, higher than expected as a stray field in the

furnace. To explain this small remanence in higher temperature ranges, we can consider two possible sources. One is chemical remanent magnetization (CRM) as an NRM carrier and the other is incomplete removal of pTRM during thermal demagnetization. However, CRM acquisition in the original firing of the pottery is ruled out by the large difference in direction between the low- and high-temperature components in some specimens (e.g., Figures 6e and 6f). CRM acquired in laboratory heatings is unlikely because no significant alteration was seen in susceptibility monitoring.

On the other hand, incomplete removal of pTRM during zero-field heating to the next temperature step is a possibility. For samples showing dual segments, there is a tendency in some samples for the NRM vector to move toward the applied field direction (shallower inclinations in vector projections). Partial TRMs acquired by PSD magnetite in previous steps may not have been completely removed in the next demagnetization steps. The effect on paleointensity is more significant for samples whose NRM direction was more or less parallel (Figure 6g) or antiparallel (Figures 6e and 6f) to the applied field direction along the furnace axis. We might expect that ~50% of the samples would show this effect, since the samples as prepared had random NRM orientations. In fact, 27 out of 49 samples show dual slopes.

The thermal demagnetization tails of pTRMs of PSD grains are rather small compared to those of MD grains [*Dunlop and Özdemir*, 2000]. Thus the change in high-temperature slope may be due to a combination of effects. In any case, only the low-temperature slopes were used in calculating paleointensities.

7.2 Comparison of VDM Results

It is interesting to compare the VADM results with other records obtained from elsewhere in North America. In Figure 8, most VADMs from the present study lie within the error limits of the reference VADMs [*Sternberg*, 1989a],

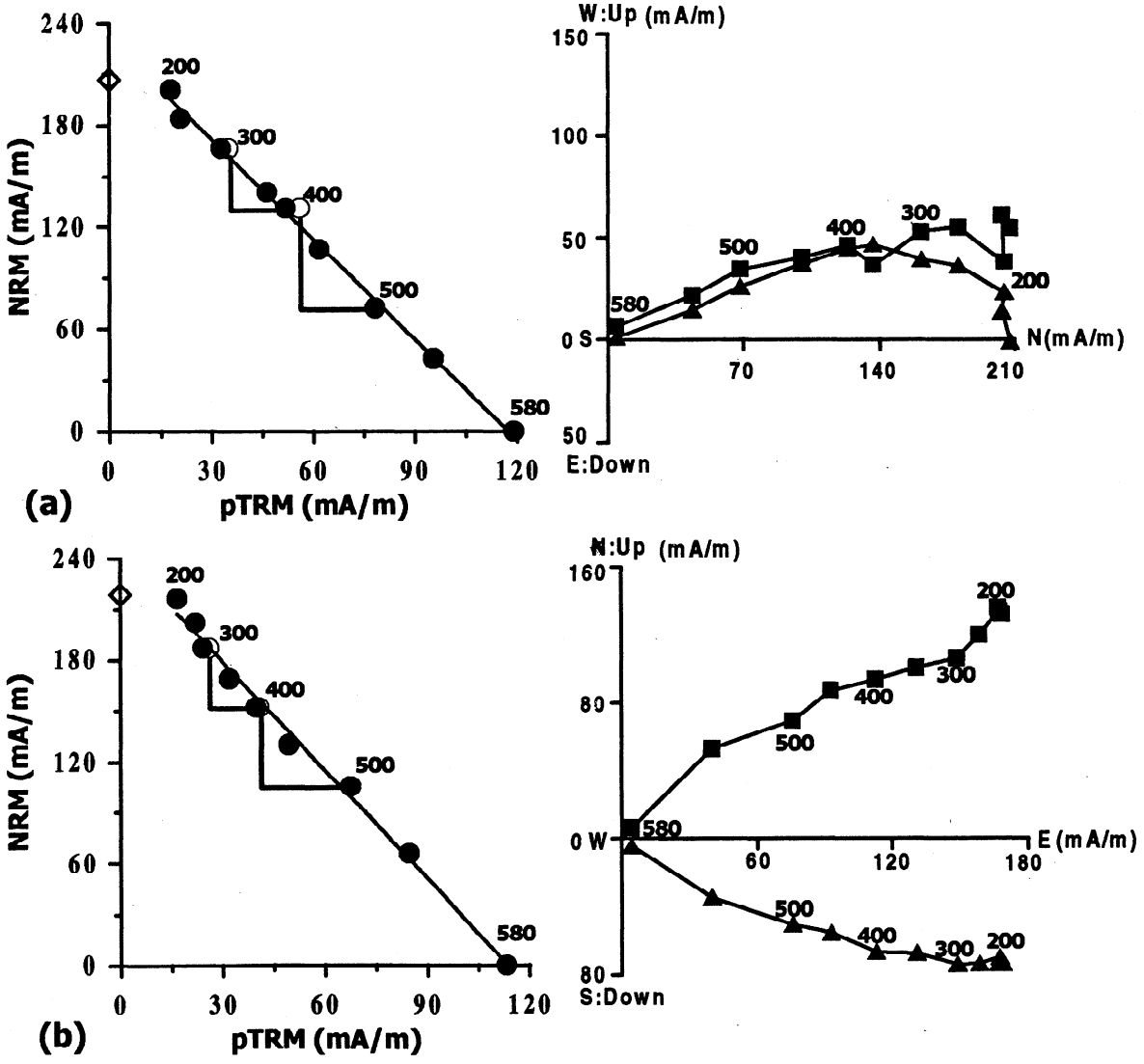

Figure 6. Remaining NRM versus acquired pTRM in double heatings to increasing temperatures (Arai plots) with associated vector projections of the NRM during thermal demagnetization for (a) SC1, (b) HB2-1, (c) SB5, (d) HL6, (e) GA15-1, (f) ER3, and (g) PB6. In NRM-TRM plots, open circles are pTRM checks at 300°C and at 400°C. Solid circles (open diamonds) represent data used (not used) in paleointensity determination. In vector projections, squares (triangles) correspond to horizontal (vertical) planes.

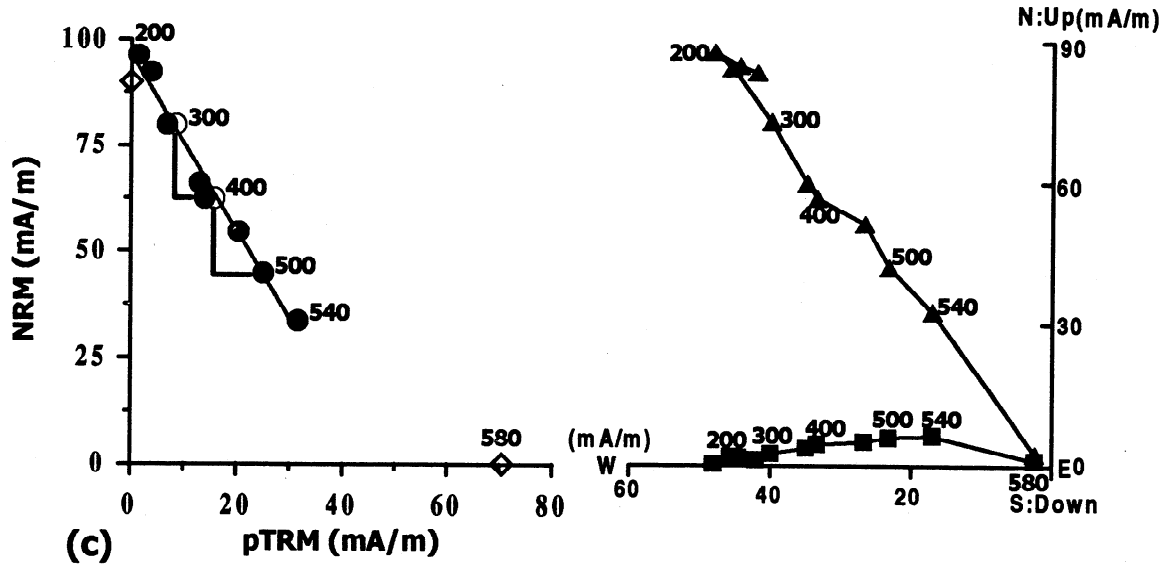

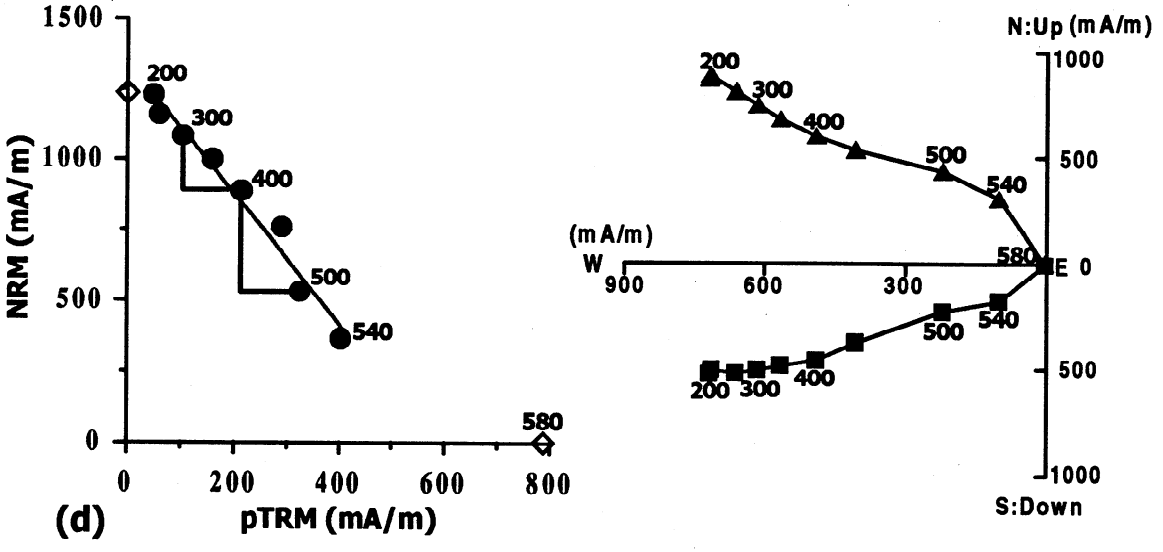

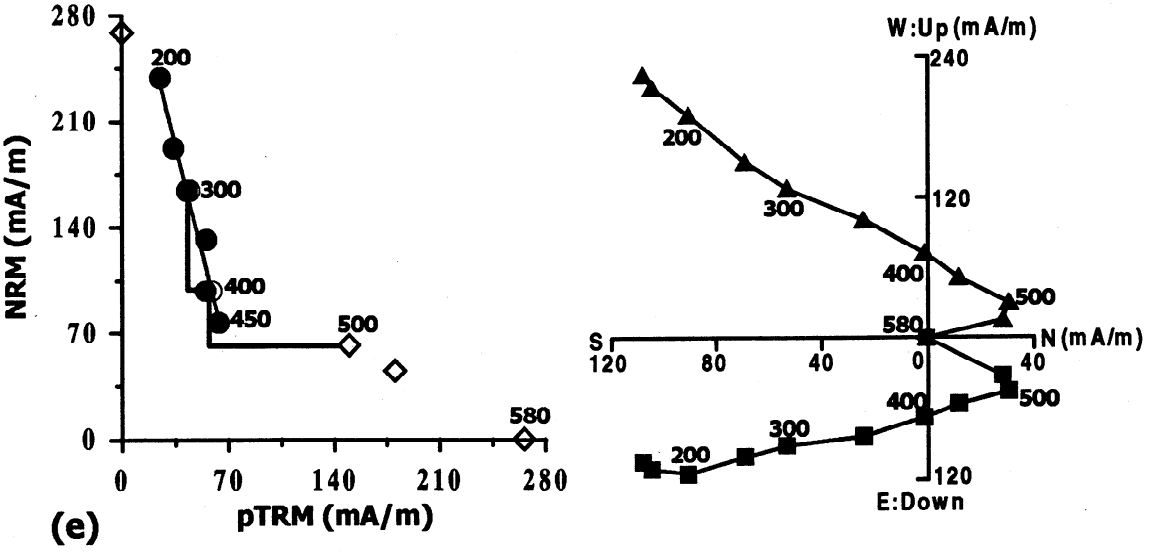

Figure 6. (continued)

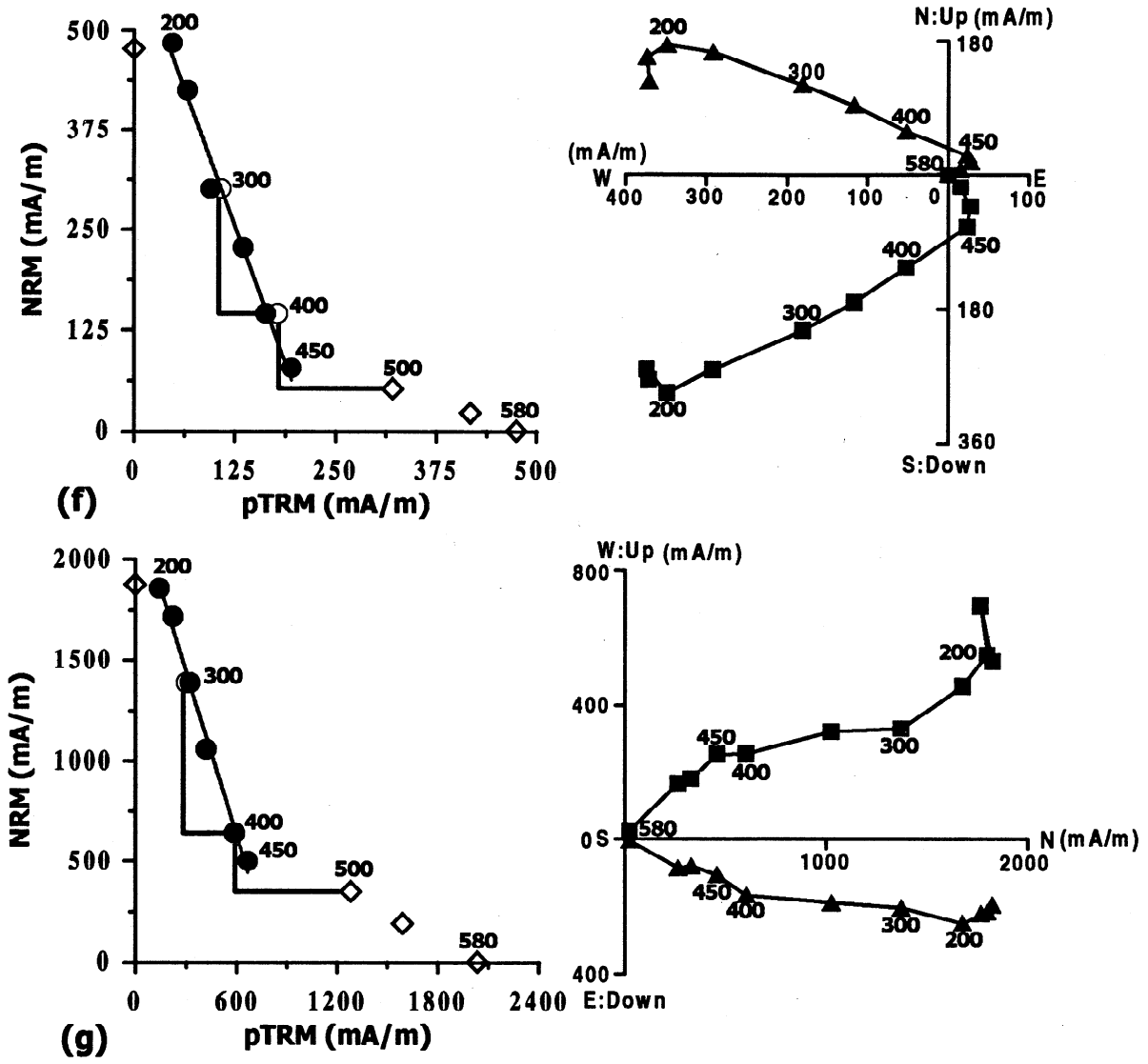

Figure 6. (continued)

although our VADMs from the tenth to the fifteenth centuries are systematically lower than values for southwestern U.S. sites. Interestingly, the VADMs of *Arbour and Schwarz* [1982] are also low in this period. Thus, within the limits represented by the error bars inherent to all the determinations, the results indicate spatial variation of VADMs in North America between ~A.D. 900 and ~A.D. 1400. It is probable that either potsherds from Ontario/Quebec or potsherds from southwestern North America have been affected by a substantial nondipole field. Although the lower Canadian VADMs have been attributed by *Sternberg* [1989a] to the effect of the ~15° latitude separation between Ontario/Quebec and the U.S. southwest, this cannot account for the difference because VADMs are values corrected for latitude.

The estimated location of the ancient north geomagnetic pole has been determined by *Ohno and Hamano* [1993] and *Hongre et al.* [1998]. A spherical harmonic model, up to degree 2 Gauss coefficients, over the past 10,000 years was established by *Ohno and Hamano* [1993]. Recently, *Hongre et al.* [1998] have updated this model, up to Gauss coefficients of degree and order 3, by using the archeomagnetic database of *Daly and Le Goff* [1996]. Interestingly, secular variation studies using oriented potsherds from Arizona show high inclinations from the tenth to the fifteenth century [*Sternberg*, 1989b] compared to the inclinations predicted by Hongre et al.'s model.

Unfortunately, there is no published continuous record of the inclination variation in Ontario/Quebec or nearby areas. We can, however, compare the inclination variation from Arizona with the results obtained from sedimentary sections in Minnesota at latitudes similar to southern Ontario. Since ~A.D. 600, a steady increase of inclination, inconsistent with the results from Arizona but similar to that of the southern Ontario results, has been measured in sediments from Lake St. Croix [*Lund and Banerjee*, 1985] and Lake Pepin [*Brachfeld*, 1999]. Thus the nondipole effect on VADMs is probably more important for southwestern North America than for Ontario/Quebec between ~A.D. 900 and ~A.D. 1400.

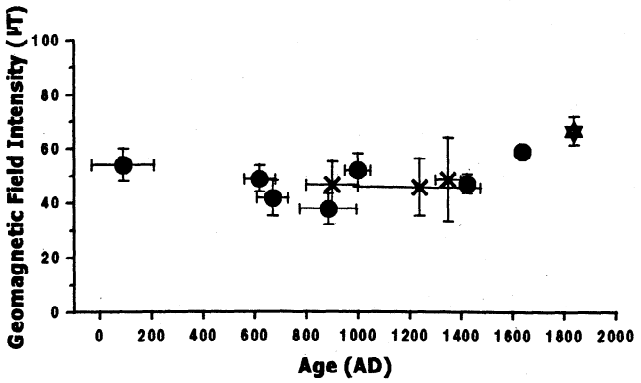

Figure 7. Geomagnetic field intensity variation for southern Ontario and Quebec. Solid circles, this study; solid star, Dunlop and Zinn [1980]; crosses, Arbour and Schwarz [1982].

7.3 Archeomagnetism as a Dating Tool

According to Figures 7 and 8, geomagnetic field intensities and the corresponding VADMs can help constrain ages of samples, although the resolution is not as good as that of the ^{14}C dating. Another problem is that paleointensity results or VADM values may not give unique ages: the Earth's magnetic field may have the same intensity at two (or more) different times (e.g., before and after the tenth century minimum in Figures 7 and 8). However, paleointensity determinations are an inexpensive supplementary dating tool in archeology.

8. Conclusions

This study demonstrates the following facts:

1. The absolute geomagnetic field intensity variation between A.D. 90 and A.D. 1640 as recorded in potsherds from Ontario was measured, with well-defined ages from ^{14}C dating, giving the first long archeomagnetic record for northeastern North America.

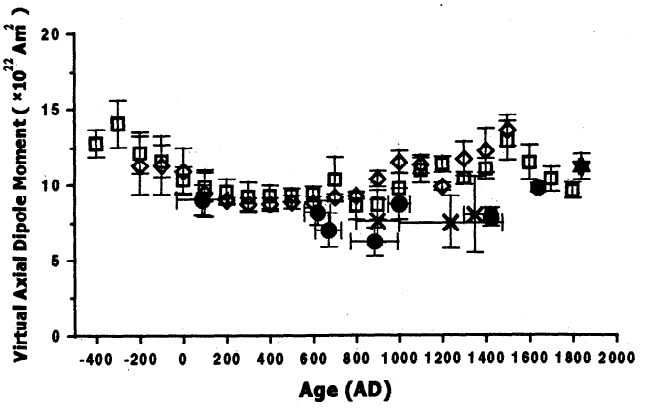

Figure 8. Comparison of VADM variations in northeastern and southwestern North America. Solid circles, this study; solid star, Dunlop and Zinn [1980]; crosses, Arbour and Schwarz [1982]; open circles, Sternberg [1989a]; open diamonds, Lee [1975], Parker [1976], and Champion [1980].

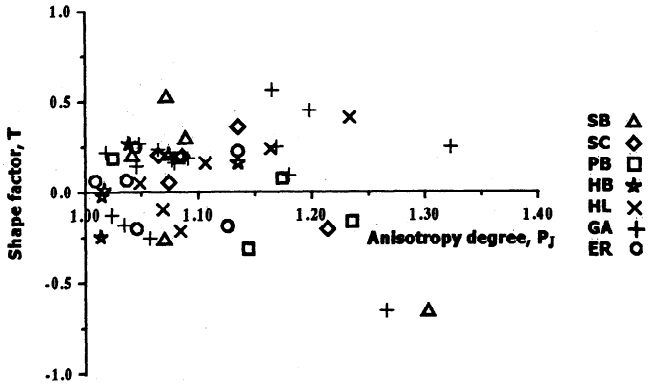

Figure 9. A plot of shape parameter T versus anisotropy degree P_J.

2. AF and thermal demagnetization, hysteresis, temperature variation of weak-field susceptibility, and microscope observations indicate that the magnetic mineralogy of the potsherds is dominated by magnetite in the PSD size range.

3. The estimated paleointensity variation shows a decrease from A.D. 90 to A.D. 885 with a subsequent increase in paleointensity to A.D. 1900.

4. The virtual axial dipole moments from the tenth to the fifteenth centuries from the present study are systematically lower than most of those in the North American database of *Sternberg* [1989a], except those of *Arbour and Schwarz* [1982] from Quebec. This difference suggests a possible contribution from nondipole fields in southwestern North America.

Appendix A: Statistical Analysis

The quality factor in slope calculation is the quantity that is being minimized in the leastsquares fitting of the bestfit

Table 4. Confidence Limits on S' Based on a Chi-Square Distribution [a]

N	n	Confidence Limit		
		99%	97.5%	95%
3	1	6.630	5.020	3.840
4	2	4.605	3.690	3.000
5	3	3.780	3.117	2.603
6	4	3.320	2.785	2.373
7	5	3.018	2.566	2.214
8	6	2.802	2.408	2.098
9	7	2.640	2.287	2.010
10	8	2.511	2.191	1.939
11	9	2.408	2.113	1.880
12	10	2.321	2.048	1.831
13	11	2.248	1.993	1.789
14	12	2.185	1.945	1.753
15	13	2.130	1.903	1.720
16	14	2.081	1.866	1.691
17	15	2.039	1.833	1.667
22	20	1.879	1.709	1.571

[a] N is the number of data points used in linear regression; n (=N-2) is the number of degrees of freedom.

line. The factor S [*York*, 1969] is the sum of the squares of the weighted deviations of the individual data points from the best-fit line:

$$S = \sum_i Z_i (y_i - bx_i - a)^2 \quad (1)$$

with

$$Z_i = \frac{w(x_i)w(y_i)}{b^2 w(y_i) + w(x_i) - 2br_i\sqrt{w(x_i)w(y_i)}}, \quad (2)$$

where x_i and y_i are the measured values, b and a are slope and extrapolated y intercept of the best fit line, $w(x_i)$ and $w(y_i)$ are the weights of the measured values, and r_i are the correlation's between the x and y errors. This quantity S has a chi-square distribution with an expectation value of N-2 where N is the total number of data points used in slope calculation. The expected value is N-2 because 2 degrees of freedom have already been used in line fitting, which requires two parameters to describe it, such as slope and y intercept. Therefore we can define a new quality factor $S' = S/(N-2)$ that has an expected value of one. Values of S' much larger than one mean that the fit is not good and that either errors were underestimated or the data points do not actually fit a straight line. The intervals used to calculate the slope in this study were selected based on the portion of the NRM-TRM data that minimizes S'. To compute a weighted paleointensity value, the weighting factor w, given by $w = fg/(\sqrt{S'}\,\sigma_a\sigma_b)$ was used where σ_a and σ_b are the standard errors in the y intercept and the slope as defined by *York* [1969].

Note that S' represents the quality of the result more precisely than the quality factor q [*Coe et al.*, 1978] or the dispersion coefficient s [*Prévot et al.*, 1985], not only because it has a statistical basis but also because we can set rejection criteria based on confidence limits. Several confidence limits on S', namely, 99%, 97.5%, and 95%, based on a chi-square distribution, are listed in Table 4. In this study we adopt a 99% confidence limit as a rejection criterion. Six results (in parentheses in Table 3) were rejected based on this criterion. For example, specimen HB7 was rejected because S' (=2.81) is larger than the reference value (=2.64) even though the specimen shows quite good quality both in f (=0.96) and g (=0.82).

Acknowledgments. Our work benefited from fruitful discussions with Derek York and Nigel Edwards. Derek York and Norm Evensen gave valuable advice on statistical approaches. Thanks to Stefanie Brachfeld for providing information regarding her sedimentary records from Lake Pepin prior to publication. Youngmin Lee provided information about thermal diffusivities of various materials. We wish to thank Mike Jackson of the Institute of Rock Magnetism (IRM) for his help with the Kappabridge measurements. Funding for the IRM is provided by the Keck Foundation, the National Science Foundation, and the University of Minnesota. Detailed reviews from Duane Champion, Andrei Kosterov, and Michel Prévot greatly improved the paper. This research has been supported by the Natural Sciences and Engineering Research Council of Canada through grant A7709 to D.J.D.

References

Aitken, M. J., A. L. Allsop, G. D. Bussell, and M. B. Winter, Geomagnetic intensity variation during the last 4,000 years, *Phys. Earth Planet. Inter.*, *56*, 49-58, 1989.

Arbour, G., and E. J. Schwarz, Archeomagnetic intensity study of Indian potsherds from Quebec, Canada, *J. Geomagn. Geoelectr.*, *34*, 129-136, 1982.

Austin, S., R. Williamson, R. Phil, and C. Short, Archaeological salvage excavation at the Scott-O'Brien (AjGv-32), City of Mississauga, Regional Municipality of Peel, Ontario, *Rep. 90WE-01*, 42 pp., Archaeol. Serv. Inc., Toronto, Ont., Canada, 1994.

Brachfeld, S. A., Separation of geomagnetic paleointensity and paleoclimate signals in sediments: examples from North America and Antarctica, Ph.D. dissertation, 245 pp., Univ. of Minn.-Twin Cities, Minneapolis, 1999.

Champion, D. E., Holocene geomagnetic secular variation in the western United States: Implications for the global geomagnetic field, *U.S Geol. Surv. Open File Rep., 80-824*, 314 pp., 1980.

Coe, R. S., Paleointensities of the Earth's magnetic field determined from Tertiary and Quaternary rocks, *J. Geophys. Res.*, *72*, 3247-3262, 1967.

Coe, R. S., C. S. Grommé, and E. A. Mankinen, Geomagnetic paleointensities from radiocarbon-dated lava flows on Hawaii and the question of the Pacific nondipole low, *J. Geophys. Res.*, *83*, 1740-1756, 1978.

Cooper, M., and D. Robertson, An archaeological assessment of proposed pit application (Varcoe pit no. 2) part of Lot 72, Concession 2, WPR township of Los, Simcoe County, Ontario, *Rep. 92VO-01*, 38 pp., Archaeol. Serv. Inc., Toronto, Ont., Canada, 1993.

Daly, L., and M. Le Goff, An updated and homogeneous world secular variation database: Smoothing of the archeomagnetic results, *Phys. Earth Planet. Inter.*, *93*, 159-190, 1996.

Day, R., M. Fuller, and V. A. Schmidt, Hysteresis properties of titanomagnetites: Grain-size and compositional dependence, *Phys. Earth Planet. Inter.*, *13*, 260-267, 1977.

Dodson, M. H., and E. McClelland Brown, Magnetic blocking temperatures for single-domain grains during slow cooling, *J. Geophys. Res.*, *85*, 2625-2637, 1980.

Dunlop, D. J., and Ö. Özdemir, *Rock Magnetism: Fundamentals and Frontiers*, 573 pp., Cambridge Univ. Press, New York, 1997.

Dunlop, D. J., and Ö. Özdemir, Effect of grain size and domain state on thermal demagnetization tails, *Geophys. Res. Lett.*, *27*, *1311-1314*, 2000.

Dunlop, D. J., and M. B. Zinn, Archeomagnetism of a 19th century pottery kiln near Jordan, Ontario, *Can. J. Earth Sci.*, *17*, 1275-1285, 1980.

Fox, J. M. W., and M. J. Aitken, Cooling-rate dependence of thermoremanent magnetization, *Nature*, *283*, 462-463, 1980.

Halgedahl, S. L., R. Day, and M. Fuller, The effect of cooling rate on the intensity of weak-field TRM in single-domain magnetite, *J. Geophys. Res.*, *85*, 3690-3698, 1980.

Hongre, L., G. Hulot, and A. Khokhlov, An analysis of the geomagnetic field over the past 2,000 years, *Phys. Earth Planet. Inter.*, *106*, 311-335, 1998.

Jackson, M., W. Gruber, J. Marvin, and S. K. Banerjee, Partial anhysteretic remanence and its anisotropy: Applications and grain size-dependence, *Geophys. Res. Lett.*, *15*, 440-443, 1988.

Jelinek, V., Characterization of the magnetic fabric of rocks, *Tectonophysics*, *79*, 63-67, 1981.

King, J. W., S. K. Banerjee, and J. Marvin, A new rockmagnetic approach to selecting sediments for geomagnetic paleointensity studies: Applications to paleointensity for the last 4000 years, *J. Geophys. Res.*, *88*, 5911-5921, 1983.

Lee, S. -S., Secular variation of the intensity of the geomagnetic field during the past 3,000 years in North, Central, and South America, Ph.D. dissertation, 200 pp., Univ. of Okla., Norman, 1975.

Levi, S., The effect of magnetite particle size on paleointensity determinations, *Phys. Earth Planet. Inter.*, *13*, 245-259, 1977.

Lund, S. P., and S. K. Banerjee, Late Quaternary paleomagnetic field secular variation from two Minnesota lakes, *J. Geophys. Res.*, *90*, 803-825, 1985.

MacDonald, R. I., and R. F. Williamson, Lennox GS x Bowmanville SS 500 kV transmission line: Archaeological mitigation at Tower 595, the Hibou site (AlGo-50), Hope Township, Northumberland County, Ontario, *Rep. 92OH-13*, 269 pp., Archaeol. Serv. Inc., Toronto, Ont., Canada, 1993.

Nagata, T., Y. Arai, and K. Momose, Secular variation of the geomagnetic total force during the last 5000 years, *J. Geophys. Res.*, *68*, 5277-5281, 1963.

Ohno, M., and Y. Hamano, Global analysis of the geomagnetic field: Time variation of the dipole moment and the geomagnetic pole in the Holocene, *J. Geomagn. Geoelectr.*, *45*, 1455-1466, 1993.

Parker, R. A., Archeomagnetic secular variation, M.S. thesis, 26 pp., Univ. of Utah, Salt Lake City, 1976.

Prévot, M., E. A. Mankinen, R. S. Coe, and C. S. Grommé, The Steens Mountain (Oregon) geomagnetic polarity transition, 2, Field intensity variations and discussion of reversal models, *J. Geophys. Res., 90*, 10,417-10,448, 1985.

Rogers, J., J. M. W. Fox, and M. J. Aitken, Magnetic anisotropy in ancient pottery, *Nature, 277*, 644-646, 1979.

Schwarz, E. J., and K. W. Christie, Original remanent magnetization of Ontario potsherds, *J. Geophys. Res., 72*, 3263-3269, 1967.

Sternberg, R. S., Archeomagnetic paleointensity in the American Southwest during the past 2,000 years, *Phys. Earth Planet. Inter., 56*, 1-17, 1989a.

Sternberg, R. S., Secular variation of archeomagnetic direction in the American Southwest, A.D. 750-1425, *J. Geophys. Res., 94*, 527-546, 1989b.

Sternberg, R. S., and R. F. Butler, An archeomagnetic paleointensity study of some Hohokam potsherds from Snaketown, Arizona, *Geophys. Res. Lett., 5*, 101-104, 1978.

Thellier, E., and O. Thellier, Sur l'intensité du champ magnétique terrestre dans le passé historique et géologique, *Ann. Geophys., 15*, 285-376, 1959.

Williamson, R. F., and R. I. MacDonald, In the shadow of the bridge; The archaeology of the Peace Bridge site (AfGr-9), 1994-1996 investigations, *1*, 526 pp., Archaeol. Serv. Inc., Toronto, Ont., Canada, 1997.

York, D., Least squares fitting of a straight line with correlated errors, *Earth Planet. Sci. Lett., 5*, 320-324, 1969.

Y. Yu, D. J. Dunlop, Geophysics, Department of Physics, University of Toronto at Mississauga, 3359 Mississauga Road North, Mississauga, Onatario, Canada L5L 1C6. (yjyu@physics.utoronto.ca; dunlop@physics.utoronto.ca)

L. Pavlish, Archaeometry Lab., University of Toronto, 60 St. George Street, Toronto, Ontario, Canada M5S 1A7. (isotrace@physics.utoronto.ca)

M. Cooper, Archaeological Services Inc., 528 Bathurst Street, Toronto, Ontario, Canada M5S 2P9. (archaeology@sympatico.ca)

(Received November 1, 1999; revised March 23, 2000; accepted May 16, 2000.)